nature plants

ARTICLES

PUBLISHED: 22 AUGUST 2016 | ARTICLE NUMBER: 16129 | DOI: 10.1038/NPLANTS.2016.129

The energetic and carbon economic origins of leaf thermoregulation

Sean T. Michaletz[1,2*], Michael D. Weiser[3], Nate G. McDowell[1], Jizhong Zhou[4,5,6], Michael Kaspari[3,7], Brent R. Helliker[8] and Brian J. Enquist[2,9,10,11]

Leaf thermoregulation has been documented in a handful of studies, but the generality and origins of this pattern are unclear. We suggest that leaf thermoregulation is widespread in both space and time, and originates from the optimization of leaf traits to maximize leaf carbon gain across and within variable environments. Here we use global data for leaf temperatures, traits and photosynthesis to evaluate predictions from a novel theory of thermoregulation that synthesizes energy budget and carbon economics theories. Our results reveal that variation in leaf temperatures and physiological performance are tightly linked to leaf traits and carbon economics. The theory, parameterized with global averaged leaf traits and microclimate, predicts a moderate level of leaf thermoregulation across a broad air temperature gradient. These predictions are supported by independent data for diverse taxa spanning a global air temperature range of ~60 °C. Moreover, our theory predicts that net carbon assimilation can be maximized by means of a trade-off between leaf thermal stability and photosynthetic stability. This prediction is supported by globally distributed data for leaf thermal and photosynthetic traits. Our results demonstrate that the temperatures of plant tissues, and not just air, are vital to developing more accurate Earth system models.

Plants are often thought to function optimally across a wide range of body temperatures that are in equilibrium with the environment[1,2]. Indeed, physiological rates, individual performance and ecosystem fluxes are all generally characterized by optimal responses to ambient air temperature[3–6]. Further, in many species, the optimal temperature for photosynthesis has shown a clear shift along with mean air temperature through a growing season and/or across elevation gradients[7–11]. On the other hand, some studies have shown that leaves may thermoregulate, so they are warmer than air in cool environments and cooler than air in warm environments[1,12–18]. When quantified by the slope of the leaf versus air temperature regression line[19], leaf thermoregulation is typically intermediate to true poikilothermy (slope of 1) and true homeothermy (slope of 0)[1,12–17]. This thermoregulation reflects a decoupling of leaf and ambient air temperatures that, if commonplace, has major implications for models of trait–climate interactions, whole-plant functioning, vegetation dynamics and ecosystem fluxes[20].

A theory of leaf thermoregulation

In this paper, we develop and evaluate a process-based theory of leaf thermoregulation. It suggests that leaf thermoregulation is widespread, and originates from selection on leaf thermal and photosynthetic traits to maximize leaf net carbon gain across variable air temperature regimes. Leaf economics theory posits that lifetime net carbon gain G is equalized by means of trade-offs of key leaf functional traits[21–23] (Fig. 1). This is formalized in equation (1), which shows that selection to maximize lifetime leaf carbon gain can be achieved in three ways: (1) increasing the time-averaged carbon assimilation rate $\langle A_a \rangle$; (2) increasing the functional leaf longevity L_f; and/or (3) decreasing the leaf mass per area (LMA)[24]. As discussed in the section 'Theoretical treatment', carbon assimilation rates vary with leaf temperature T_l (ref. 8), and leaf temperature variation is governed by an interaction of leaf traits (the thermal time constant τ) and climate variables within leaf energy budgets. Consequently, energy budgets provide a mechanistic framework for linking leaf functional traits, thermoregulation and carbon economics in both space and time.

Leaf thermoregulation in space can be characterized using a steady-state energy budget (for example, equation (2)). Combined with carbon economics theory (equation (1)), this energy budget predicts that thermoregulation may originate from selection on leaf thermal and photosynthetic traits to maintain leaf temperatures that are optimal for photosynthesis[9,10,25]. Indeed, maintenance of leaf temperatures around a photosynthetic optimum has recent empirical support[26,27]. This would serve to increase $\langle A_a \rangle$ and help maximize G. Understanding thermoregulation in time is more complicated. Since time-averaged leaf temperatures during periods when most photosynthesis occurs will be approximately equal to the optimal temperature for photosynthesis[9,10,25–27], selection to maximize G should then favour leaf traits that yield temporal leaf temperature variation of a magnitude similar to the thermal breadth of photosynthesis T_{90} (the temperature range where assimilation rates are $\geq$ 90% of their maximum value; Supplementary Fig. 1). Temporal variation in leaf temperature (thermal stability) is governed by the thermal time constant τ (s), a composite leaf trait comprising several additional functional traits[1] (equation (7)). If G is maximized using τ and its constituent traits, then variation in these traits reflects the capacity for selection to influence leaf

[1]Earth and Environmental Sciences Division, Los Alamos National Laboratory, MS J495, Los Alamos, New Mexico 87545, USA. [2]Department of Ecology and Evolutionary Biology, University of Arizona, Tucson, Arizona 85721, USA. [3]Department of Biology, EEB Graduate Program, University of Oklahoma, Norman, Oklahoma 73069, USA. [4]Institute for Environmental Genomics, and Department of Microbiology and Plant Biology, University of Oklahoma, Norman, Oklahoma 73019, USA. [5]State Key Laboratory of Environment Simulation and Pollution Control, School of Environment, Tsinghua University, Beijing 100084, China. [6]Earth Science Division, Lawrence Berkeley Laboratory, Berkeley, California 94270, USA. [7]Smithsonian Tropical Research Institute, Balboa, Republic of Panama. [8]Department of Biology, University of Pennsylvania, Philadelphia, Pennsylvania 19104, USA. [9]The Santa Fe Institute, 1399 Hyde Park Rd, Santa Fe, New Mexico 87501, USA. [10]The iPlant Collaborative, Thomas W. Keating Bioresearch Building, 1657 East Helen Street, Tucson, Arizona 85721, USA. [11]Aspen Center for Environmental Studies, 100 Puppy Smith Street, Aspen, Colorado 81611, USA. *e-mail: michaletz@lanl.gov

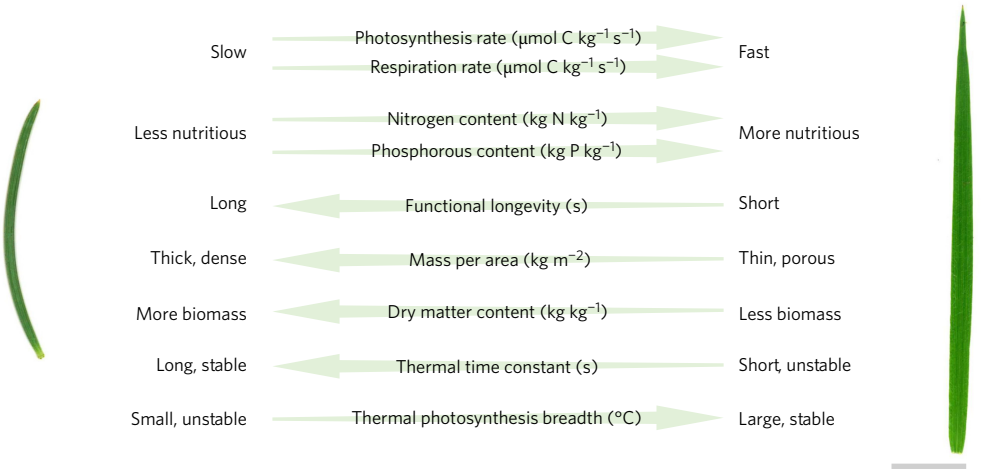

Figure 1 | Leaf thermal traits and the leaf economics spectrum. General relationships between leaf traits suggest that the global leaf economics spectrum[21,22] reflects not only carbon economics, but also the energetic processes that govern them. For example, as formalized in equations (6)–(8), LMA, LDMC and τ play fundamental mechanistic roles in thermal buffering and thus net carbon gain of a leaf. The 'slow' strategy is illustrated by *Pinus edulis* (LMA = 0.41 kg m^{-2}, τ = 41.22 s) and the 'fast' strategy is illustrated by *Brachypodiuum distachyon* (LMA = 0.03 kg m^{-2}, τ = 1.56 s). LMA and τ were calculated from global trait databases[22,28]. Scale bar, 1 cm.

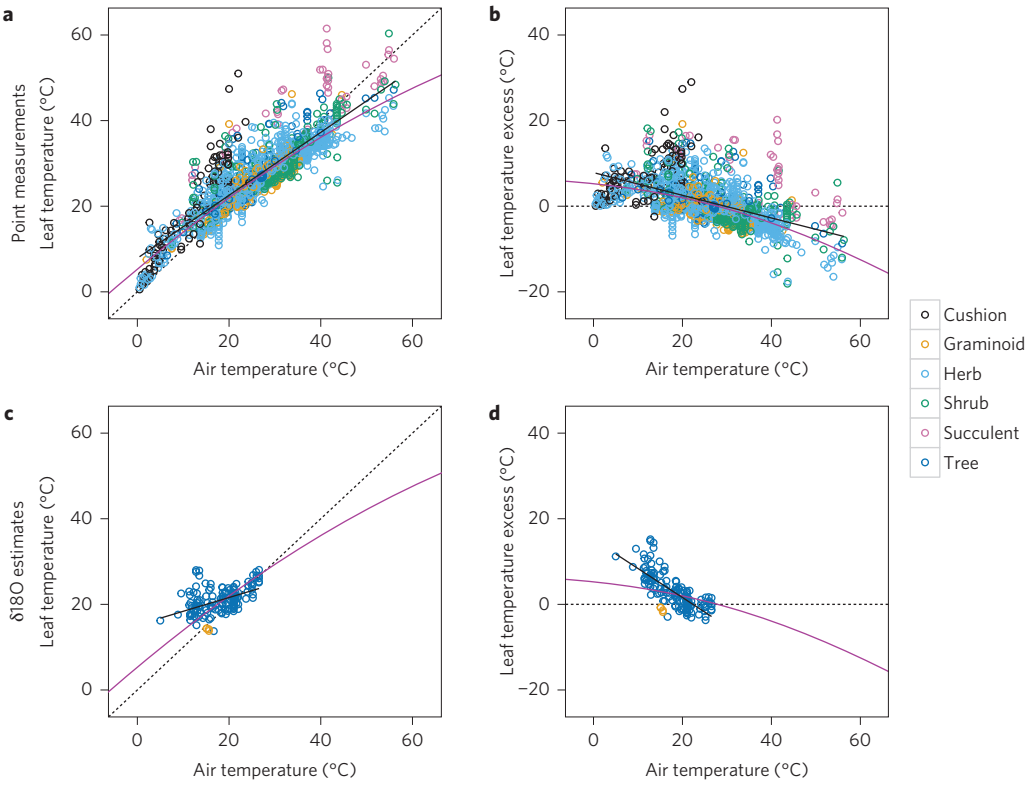

Figure 2 | Leaf thermoregulation across global air temperature gradients. The panels compare a steady-state energy budget prediction with empirical data estimated by two methods. To assist comparison, the non-linear relationships predicted by the energy budget solution of Supplementary Equations (16)–(25) were fitted using OLS regression across the range of observed air temperatures. **a**,**b**, Temperatures from short-term point measurements of 1,504 individual leaves from 185 taxa. For leaf temperature (**a**), the fitted slope of 0.74 (r^2 = 0.74) is greater than 0 ($P < 2.2 \times 10^{-16}$) and less than 1 ($P < 2.2 \times 10^{-16}$), and the 95% CI (0.71–0.76) almost includes the energy budget prediction of 0.70. For leaf temperature excess ($T_l - T_a$; **b**), the fitted slope of −0.27 (r^2 = 0.27) is less than 0 ($P < 2.2 \times 10^{-16}$) and greater than −1 ($P < 2.2 \times 10^{-16}$), and the 95% CI (−0.29 to −0.24) almost includes the energy budget prediction of −0.30. **c**,**d**, Temperatures from long-term, photosynthetically weighted estimates based on cellulosic δ^{18}O for over 64 species of trees and graminoids. For δ^{18}O leaf temperature (**c**), the fitted slope of 0.32 (r^2 = 0.23) is greater than 0 ($P < 5.77 \times 10^{-10}$) and less than 1 ($P < 2.2 \times 10^{-16}$), and the 95% CI (0.23–0.42) does not include the energy budget prediction. For δ^{18}O leaf temperature excess (**d**), the fitted slope of −0.68 (r^2 = 0.57) is less than 0 ($P < 2.2 \times 10^{-16}$) and greater than −1 ($P < 2.2 \times 10^{-16}$), and the 95% CI (−0.77 to −0.58) does not include the energy budget prediction. Taxa and primary sources for all data are given in the Supplementary Information. Black solid lines, OLS regression; pink solid lines, steady-state energy budget prediction (Supplementary Equations (16)–(25) parameterized with global average traits[22,28] and microclimate[29]); black dashed lines, true poikilothermy ($T_l = T_a$).

temperatures and carbon gain. However, maximization of G appears to be limited by two important trait trade-offs. First, LMA varies directly with L_f (refs 21,22), showing that leaves cannot simultaneously increase L_f and decrease LMA (Fig. 1). Second, all else equal, LMA should vary directly with $\langle A_a \rangle$, because it is directly related to τ (equation (7)) and assimilation rate (assuming leaf temperature oscillation about a photosynthetic optimum, as has recently been shown[26,27]; see section 'Theoretical treatment'). Since these trade-offs will constrain G, any mechanism that reconciles them should confer a selective advantage. Our theory predicts that a trade-off between thermal stability and photosynthetic stability (i.e. an inverse relationship between τ and T_{90}) enables leaves to simultaneously increase $\langle A_a \rangle$ and decrease LMA, helping to maximize G despite correlated trade-offs that would otherwise constrain G.

Theoretical treatment

We propose that leaf thermoregulation helps to maximize the instantaneous, time-averaged and lifetime net carbon gain of leaves[1]. This can be expressed in terms of several key functional traits as[1,23,24,32]

$$G = \frac{A_{tot}}{LMA} \cdot \frac{k_1}{k_2} = \frac{\int_{t=0}^{L_f} A_a(t)dt}{LMA} \cdot \frac{k_1}{k_2} \approx \frac{\langle A_a \rangle L_f}{LMA} \cdot \frac{k_1}{k_2} = \langle A_m \rangle L_f \cdot \frac{k_1}{k_2} \geq 1 \quad (1)$$

where G is lifetime net carbon gain per unit carbon invested (kg C kg C^{-1}), A_{tot} is the cumulative net carbon assimilated throughout the life of the leaf (μmol C m^{-2} s^{-1}), LMA is the leaf mass per area (kg m^{-2}), k_1 is the molar mass conversion factor (kg C μmol C^{-1}), k_2 is the carbon mass fraction (kg C kg^{-1}), A_a is the time-averaged net carbon assimilation rate per unit leaf area (μmol C m^{-2} s^{-1}), $\langle A_a \rangle$ is the time-averaged net carbon assimilation rate per unit leaf area (μmol C m^{-2} s^{-1}), L_f is the functional leaf longevity (s), and $\langle A_m \rangle$ is the time-averaged net carbon assimilation rate per unit leaf mass (μmol C kg^{-1} s^{-1}). Additional derivations and definitions needed to elaborate this and the following equations are included in the Supplementary Information. Inspection of equation (1) shows that G could be maximized by selection to increase A_{tot}, increase $\langle A_a \rangle$, increase L_f, and/or decrease LMA[24].

Selection to increase $\langle A_a \rangle$ could operate on leaf photosynthetic and thermal traits to help maintain average leaf temperatures near those that are optimal for photosynthesis[9–11,25–27]. Leaf temperatures can be predicted from leaf traits and climate by solving the steady-state energy budget of Supplementary Equation (11) (see Supplementary Information; refs 43–46). One simple approach is the Penman approximation (Supplementary Equation (12)), which solves Supplementary Equation (11) to give

$$T_l = T_a + \frac{R\gamma\left[g_{b,h}/g_w\right]}{\rho_a c_p g_{b,h}\left[s + \gamma\left[g_{b,h}/g_w\right]\right]} - \frac{D}{s + \gamma\left[g_{b,h}/g_w\right]} \quad (2)$$

or

$$T_l - T_a = \frac{R\gamma\left[g_{b,h}/g_w\right]}{\rho_a c_p g_{b,h}\left[s + \gamma\left[g_{b,h}/g_w\right]\right]} - \frac{D}{s + \gamma\left[g_{b,h}/g_w\right]} \quad (3)$$

where T_l (K) is the leaf temperature, T_a (K) is the air temperature, $T_l - T_a$ (K) is the leaf temperature excess, R (W m^{-2}) is the net radiation flux (Supplementary Equation 3), γ (Pa K^{-1}) is the psychrometric constant (Supplementary Equation 9), $g_{b,h}$ (m s^{-1}) is the boundary layer conductance to heat (Supplementary Equations 5 and 6), g_w (m s^{-1}) is the water vapour conductance (Supplementary Equation 8), ρ_a (kg m^{-3}) is the density of air, $c_{p,a}$ (J kg^{-1} K^{-1}) is the specific heat capacity of air, s (Pa K^{-1}) is the slope of the saturation vapour pressure curve versus temperature evaluated at T_a, and D (Pa) is the vapour pressure deficit. By setting the leaf temperature excess to zero and simplifying, the theoretical equivalence point temperature can be expressed as[31]

$$T_{eq} \equiv T_l = T_a = \left[R_{abs} - \frac{\rho_a c_{p,a} g_w D}{\gamma}\right]^{1/4} \left[\frac{\varphi}{\varepsilon\sigma}\right]^{1/4} \quad (4)$$

where R_{abs} (W m^{-2}) is the incident radiation absorbed by the leaf, ϕ (dimensionless) is the ratio of projected-to-total leaf area, ε (dimensionless) is the leaf emissivity, and σ (W m^{-2} K^{-4}) is the Stefan–Boltzmann constant. If selection acts to maintain average temperatures near photosynthetic optima, then we hypothesize that the theoretical equivalence point temperature should be approximately equal to the optimal temperature for photosynthesis ($T_{eq} \approx T_{opt}$).

In equation (3), the first term on the right describes a contribution to the leaf temperature excess that is proportional to net radiation, whereas the second term describes a contribution that is proportional to the vapour pressure deficit. Depending on the relative magnitudes of these terms, leaf temperature will be warmer than, cooler than, or equivalent to air temperature. Thus, equations (2)–(4) show how leaf thermoregulation can emerge from an interaction of leaf thermal traits (absorptivity, emissivity, size, geometry and stomatal conductance) and climate variables within leaf energy budgets. The thermal traits governing leaf temperatures and thermoregulation vary directionally across air temperature gradients[33,34]. Even so, all else equal, the first term in equation (3) will dominate in low air temperatures because s and D decrease with temperature, yielding leaf temperatures that are warmer than air. Conversely, the second term will dominate in high air temperatures because D increases with temperature, resulting in leaf temperatures that are cooler than air.

Equation (2) links leaf traits and climate to rates of net photosynthesis, which are temperature-dependent (Supplementary Equations (28)–(33)). Since photosynthesis rate $\langle A_a \rangle$ is maximized when leaf temperature equals the optimal temperature for photosynthesis ($T_l = T_{opt}$), we can rewrite Supplementary Equation (41) for T_{opt} to give Supplementary Equation (45). Substituting Supplementary Equation (45) into equation (1) yields a simple expression linking leaf carbon economics, functional traits, and steady-state energy budgets

$$G = \frac{\left[aT_{opt}^2 + bT_{opt} + c\right]L_f}{LMA} \cdot \frac{k_1}{k_2} \geq 1 \quad (5)$$

where again $\langle A_a \rangle$ may maximized via the photosynthetic trait T_{opt} and/or leaf thermal traits within the leaf energy budget of equation (2). Thus, equations (2)–(5) (and additional theory detailed in the Supplementary Information) formalize how key leaf traits such as the temperature optima of photosynthesis, absorptivity, angle, size, geometry, and stomatal conductance can govern leaf thermoregulation and maximization of G across climate gradients.

G could also be maximized by selection to increase A_{tot} via functional traits that help maintain time-dependent leaf temperatures near photosynthetic optima[1,25–27,35,36]. If we assume a sinusoidally oscillating environment (Supplementary Equation (29)), Supplementary Equation (26) can be solved to give the transient leaf temperature as

$$T_l = \bar{T}_e + \frac{\Delta T_e}{1 + \left[2\pi f\tau\right]^2}\left[\sin(2\pi ft) - 2\pi f\tau\cos(2\pi ft)\right] \quad (6)$$

where $\bar{T}_e$ (K) is the mean equilibrium leaf temperature, ΔT_e (K) is the amplitude of oscillation in equilibrium temperature, f (Hz)

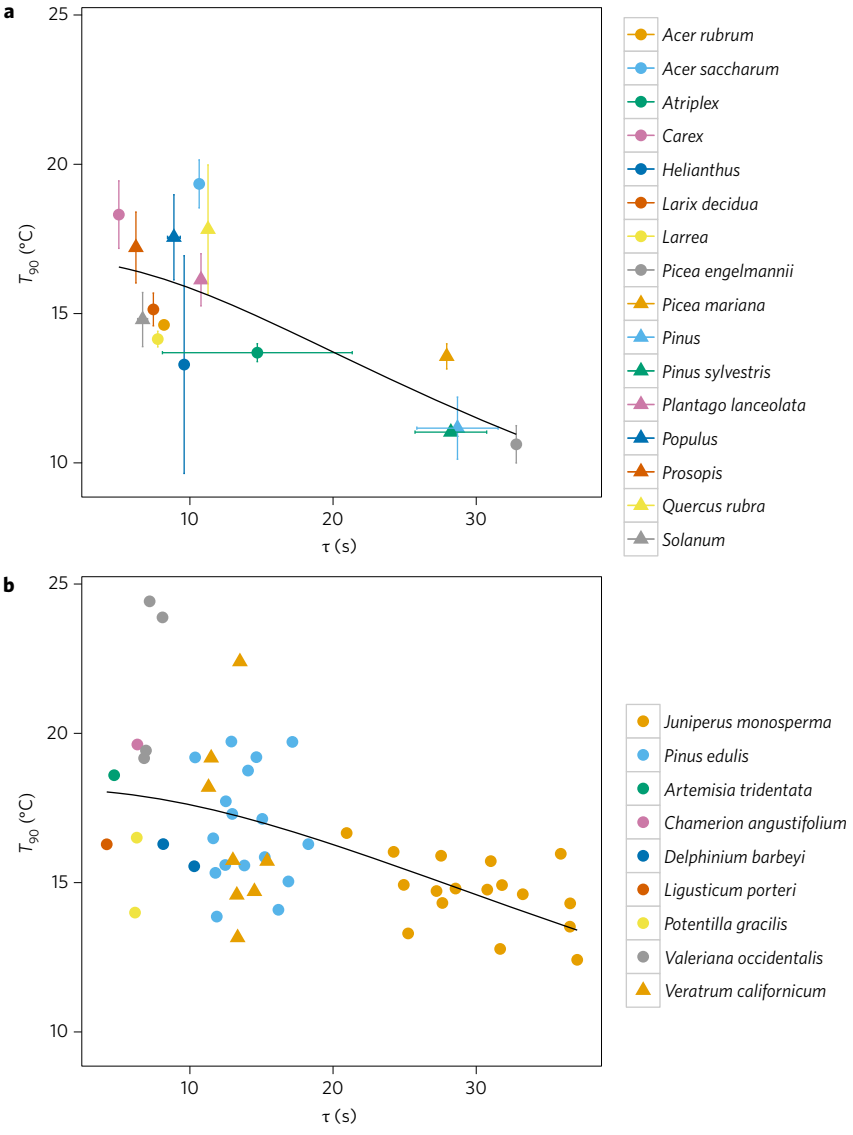

Figure 3 | Relationship between T_{90} and τ. In support of our theory, inverse relationships between T_{90} and τ were observed. The residual variation in T_{90} (Supplementary Equation (44)) probably reflects the use of simple second-order polynomials (Supplementary Equation (41)) to characterize the temperature response of net photosynthesis. **a**, Means ± 1 standard error calculated from published data for 16 taxa ($r^2 = 0.59$, $P_{\Delta T_e} = 1.25 \times 10^{-12}$, $P_f = 1.29 \times 10^{-4}$). Data used to calculate T_{90} and τ were not measured on the same leaves. Primary data sources are listed in the Supplementary Information. **b**, Original data for 62 leaves from nine species ($r^2 = 0.30$, $P_{\Delta T_e} < 2 \times 10^{-16}$, $P_f = 1.55 \times 10^{-8}$). These data are unique in that traits needed to estimate T_{90} and τ were measured on the same leaves. Solid black line, non-linear regression of Supplementary Equation (50); error bars, ±1 standard error.

is the frequency, and t (s) is time. The thermal time constant τ (s) is a composite trait that quantifies the thermal stability of a leaf

$$\tau = \varphi LMA\left[\frac{c_{p,w}}{LDMC \cdot h} + \frac{c_{p,d} - c_{p,w}}{h}\right] \quad (7)$$

Here, ϕ (dimensionless) is the ratio of projected-to-total leaf area, LMA (kg m^{-2}) is the leaf mass per area (m^2), LDMC is the leaf dry matter content (kg kg^{-1}), h (W m^{-2} K^{-1}) is an overall heat transfer coefficient (Supplementary Information) and $c_{p,d}$ (J kg^{-1} K^{-1}) and $c_{p,w}$ (J kg^{-1} K^{-1}) are the specific heat capacities of dry leaf matter and water, respectively. Small thermal time constants correspond to leaves that respond rapidly to changes in environmental temperature, whereas large thermal time constants correspond to leaves that respond slowly to changes in environmental temperature (equation (6); Supplementary Fig. 4; Fig. 3 in ref. 1). From Supplementary Equation (48), temperature-dependent photosynthesis rates are integrated over L_f to give A_{tot}; substituting into equation (1) gives

$$G = \frac{\int_{t=0}^{L_f} A(T_l(t))dt}{LMA} \cdot \frac{k_1}{k_2} \approx \frac{\langle A_a \rangle L_f}{LMA} \cdot \frac{k_1}{k_2} \geq 1 \quad (8)$$

where the transient leaf temperature $T_l(t)$ is governed by leaf traits and climate variables from equations (6) and (7).

The ability of leaves to maximize G in equation (8) appears to be restricted by two functional trait trade-offs. First, LMA varies directly with L_f[21,22], demonstrating that leaves generally cannot increase L_f while decreasing LMA (Fig. 1). Second, all else equal, LMA should vary directly with $\langle A_a \rangle$ because thermal stability should promote photosynthetic stability (Supplementary Information; ref. 1). However, a trade-off between thermal stability and photosynthetic stability could enable leaves to increase $\langle A_a \rangle$ while decreasing LMA. Photosynthetic stability is quantified by the thermal

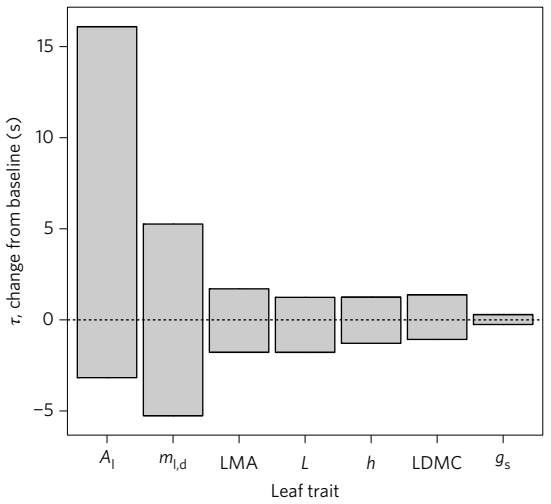

Figure 4 | Sensitivity of leaf thermal time constants τ to variation in seven constituent leaf traits. The baseline time constant was calculated using median values of traits from global trait databases[22,28], and upper and lower bounds for each leaf trait were taken as the median ± 0.5 median absolute deviation of leaf trait data. The same general results were observed when using median ± minimum and maximum observed values. This analysis suggests that leaf thermal time constants are most sensitive to variation in total leaf area A_l, followed by dry leaf mass $m_{l,d}$, LMA, leaf characteristic dimension L, heat transfer coefficient h, LDMC and stomatal conductance g_s.

breadth of photosynthesis T_{90} (K; the temperature range where the photosynthesis rate is ≥90% of maximum; Supplementary Fig. 1). If selection operates on T_{90} and τ to maximize instantaneous photosynthesis rates, then T_{90} should be proportional to the realized peak-to-peak amplitude of leaf temperature $2\Delta T_e'$(K), which is a function of τ. From Supplementary Equations (19) and (20), this can be formalized as

$$T_{90} \propto 2\Delta T_e' = 2\Delta T_e \cos\left(\tan^{-1}\left(2\pi f \tau\right)\right) \quad (9)$$

Thus, equation (9) predicts an inverse relationship between τ and T_{90}. This trade-off between τ and T_{90} enables leaves to maximize A_{tot}, $\langle A_a \rangle$, and L_f while minimizing LMA because it helps maintain leaf temperature variation within the thermal breadth of photosynthesis.

Results

A predicted general leaf thermoregulation is supported by global temperature data. We evaluate our steady-state theory for leaf thermoregulation by testing predictions for (1) short-term leaf temperature versus air temperature and (2) long-term leaf temperature versus air temperature. We employ a 'zeroth order' approach intended to evaluate the general thermoregulatory response of a global average leaf. We purposely do not consider complexities such as how trait variation leads to residual variation around the general relationship, although the theory can be used to address such questions provided that necessary data are available for parameterization. Thus, we begin by parameterizing the steady-state energy budget of Supplementary Equations (16)–(25) for a typical leaf based on global average leaf traits[22,28] and microclimate[29,30]. All trait and climate averages were held constant, except for air temperature. Across an air temperature gradient from 0 to 60 °C, Supplementary Equations (16)–(25) predict that (1) leaf temperature will almost never equal ambient air temperature, and (2) leaf temperature plotted on air temperature will have an approximately linear relationship with a slope of 0.70 and a general leaf–air equivalence point temperature ($T_{eq} = T_l = T_a$) of 27.75 °C (but see Supplementary Information and ref. 31) so that $T_l = 13.99$ °C at $T_a = 10$ °C, and $T_l = 41.57$ °C at $T_a = 50$ °C.

To assess these predictions, we compiled short-term point temperature data for 1,504 sunlit leaves from 185 taxa spanning approximately 60 °C of air temperature (data are described in Supplementary Information). Short-term point measurements are most appropriate for evaluating steady-state predictions, because they have not been adjusted to account for the physiological status of the leaf (as in the $\delta^{18}O$ approach[16] described below). These data provide strong support for the steady-state theory (Fig. 2a,b; root mean squared error (r.m.s.e.) = 4.45, normalized root mean squared error (n.r.m.s.e.) = 0.07). First, leaves are not poikilothermic and their temperatures rarely equal ambient air temperatures. The fitted slope of 0.74 ($r^2 = 0.74$; Fig. 2a) is significantly greater than 0 ($P < 2.2 \times 10^{-16}$) as required for true homeothermy and significantly less than 1 ($P < 2.2 \times 10^{-16}$) as required for true poikilothermy. The slope has a narrow 95% CI (0.71–0.76) that almost includes the general energy budget prediction of 0.70. Second, the observed T_{eq} of 29.64 °C is close to the energy budget prediction reported above. Third, leaf temperatures estimated from the fitted regression give $T_l = 15.20$ °C (95% CI = 14.37–16.03 °C) at $T_a = 10$ °C, and $T_l = 44.61$ °C (95% CI = 42.90–46.31) at $T_a = 50$ °C, which almost include the energy budget predictions reported above.

It is important to note that there is substantial residual variation around this general relationship (Fig. 2a,b), indicating that some leaves can differ dramatically from the prediction of our steady-state analysis. As discussed in the section 'Theoretical treatment', leaf thermoregulation reflects an increase of leaf temperature above cool air because of increased net radiation and/or decreased evaporative cooling, and a decrease of leaf temperature below warm air because of decreased net radiation and/or increased evaporative cooling. Equations (2) and (3) show how leaf thermoregulation is governed by leaf thermal traits (absorptivity, emissivity, size, geometry and stomatal conductance) and climate variables, and there is strong indication that departures from the general relationship result from variation in leaf traits and growth form (Fig. 2 and Supplementary Fig. 2). Indeed, thermoregulation patterns vary among plant growth forms (Supplementary Information, Supplementary Fig. 2 and Supplementary Tables 1–3). Graminoids and shrubs showed the smallest departure of leaf temperature from air temperature, followed by herbs and trees, and finally succulents and cushions (Supplementary Fig. 2 and Supplementary Table 3). Leaf temperatures of cushion plants were always warmer than and increased with air temperature (Supplementary Fig. 2), which is likely to reflect adaptive morphologies and statures that promote warming in the cold arctic and montane areas that they occupy.

Next, we assessed long-term metabolic temperatures of leaves. We compiled photosynthetically weighted leaf temperature data that were estimated for more than 64 species using a cellulose $\delta^{18}O$ model parameterized for tree wood and graminoid leaves (data are described in Supplementary Information). These $\delta^{18}O$ estimates provide a more time-integrated measure of the average temperature at which net photosynthesis is most productive. Regression again revealed a thermoregulation of leaves (slope = 0.32, $r^2 = 0.23$; Fig. 2c) that was intermediate to true homeothermy ($P < 5.77 \times 10^{-10}$) and true poikilothermy ($P < 2.2 \times 10^{-16}$). However, the fitted slope (95% CI = 0.23–0.42) was significantly *less* than the steady-state prediction of Supplementary Equations (16)–(25), indicating that leaf metabolism is optimized at temperatures much closer to true homeothermy (a slope of 0). Thus, although broadly consistent with the point measurements, $\delta^{18}O$ estimates differ in two important ways. First, the slope is shallower, because $\delta^{18}O$ leaf temperature estimates primarily reflect leaf temperatures that are optimal for photosynthesis. Second, the leaf–air equivalence point temperature T_{eq} of 22.36 °C is lower, because the $\delta^{18}O$ approach integrates shaded and unshaded

leaves whereas the point data are biased towards sunlit leaves (see Methods). This deviation of long-term $\delta^{18}O$ leaf temperatures from Supplementary Equations (16)–(25) predictions (r.m.s.e. = 3.43, n.r.s.m.e. = 0.24) is a manifestation of temporal variation in leaf temperatures and carbon assimilation rates, which cannot be captured in a steady-state theory.

A predicted trade-off of thermal and photosynthetic stability traits is supported by global trait data. The transient version of our theory shows how time-dependent leaf temperatures and assimilation rates are governed by key leaf thermal and photosynthetic traits (equations (6)–(9)). Specifically, it predicts that a trade-off between traits regulating variation in temperature (τ) and assimilation rates (T_{90}) enables leaves to maximize net carbon gain. To evaluate this prediction, we examine globally distributed data for τ and T_{90} compiled from the literature (described in Supplementary Information) and collected along an air temperature gradient in the western USA. Values of τ and T_{90} did not vary significantly between C3 and C4 plants ($P = 0.50$ and 0.06, respectively), although this test is not comprehensive since almost all of our data are for C3 species (see Supplementary Information).

In support of our theory, inverse relationships were observed between T_{90} and τ (Fig. 3), as quantified by non-linear regression of Supplementary Equation (50) for literature data ($r^2 = 0.59$, $P_{\Delta T_e'} = 1.25 \times 10^{-12}$, $P_f = 1.29 \times 10^{-4}$) and measured data ($r^2 = 0.30$, $P_{\Delta T_e'} < 2 \times 10^{-16}$, $P_f = 1.55 \times 10^{-8}$). This trade-off enables thermally unstable leaves to maintain relatively stable rates of instantaneous net photosynthesis, which helps maximize the time-averaged rate of photosynthesis as well as total lifetime carbon gain G. This is important given that our observed variation in τ corresponds to substantial variation in leaf thermal response for typical outdoor environments (Supplementary Fig. 4). Indeed, simulations using Supplementary Equations (14)–(21) and Supplementary Equations (34)–(36) parameterized with our data predict that G is approximately invariant with functional leaf longevity (Supplementary Fig. 4d), which is consistent with theory and data for leaf economics[32]. Residual variation in T_{90} appeared to decrease with τ, which may reflect the smaller number of data or smaller diversity of taxa having larger values of τ in our dataset. Together, these results highlight τ as a key leaf carbon economics trait. Since τ comprises several additional functional traits (equation (7)), it is likely that the global leaf economics spectrum[21,22] reflects not only carbon economics, but also the energetic processes that govern them. For example, equation (7) formalizes the roles of LMA and leaf dry matter content (LDMC) in buffering leaf temperature variation. This can help maintain leaf temperatures near metabolic optima and maximize rates of net carbon assimilation.

Variation in τ is rooted in variation of its constituent traits. Since τ influences dynamics of leaf temperature and assimilation rates (Supplementary Fig. 3b,c), then variation in these traits reflects the capacity for selection to influence leaf temperature and assimilation. To evaluate how variation in leaf traits influences variation in thermal time constants, we conducted a sensitivity analysis of equation (7) (Fig. 4). The results suggest that variation in τ is most sensitive to variation in total surface area and dry mass, and only moderately sensitive to variation in LMA, width, the overall heat transfer coefficient and LDMC. Variation in stomatal conductance had little influence on τ. We conclude that leaf surface area and dry mass offer the most phenotypic variation on which natural selection may act to buffer leaf temperature variation and maximize leaf carbon gain.

Discussion

We propose that leaf thermoregulation originates from selection on leaf traits to maximize carbon gain in space and time. Our energy budget analysis predicted leaf thermoregulation across a global air temperature gradient. This prediction was supported by independent leaf temperature data estimated using two different methods (Fig. 2). Our theory also correctly predicted the inverse relationship between leaf thermal traits and the thermal breadth of photosynthesis, highlighting a key trade-off between leaf thermal and photosynthetic stability (Fig. 3). This trade-off appears common to all leaves, and probably underlies how natural selection has shaped the diversity of leaf form and function across climates to maximize the lifetime net carbon gain of leaves. Leaf area and dry mass appear to be central thermal traits that provide most of the variation on which natural selection may act to influence buffering of leaf temperatures and assimilation rates (Fig. 4). However, several other traits often studied in trait-based ecology also appear to be important. Our theory provides a key step in developing a more quantitative plant ecology capable of addressing several long-standing questions in the evolution of plant form, function, and diversity. For example, further elaborations of the theory can mechanistically examine (1) the relative importance of time-averaged versus maximum net photosynthesis rates for lifetime carbon gain in leaves subjected to real-world environmental variation, (2) how covariation and diversity of multiple leaf traits across climate gradients may influence leaf thermoregulation, and (3) how anticipated climate change scenarios may change the suite of leaf thermal and photosynthetic traits that are favoured at a given site. As it stands, our results shed new light on the mechanisms linking leaf traits, temperature, temperature variation and carbon economics. Further, our theory and empirical data demonstrate that future studies need to consider *both* leaf and air temperatures.

Methods

Leaf thermoregulation data. We evaluated empirical evidence for leaf thermoregulation using leaf and air temperature data estimated using two different approaches. First, short-term point measurements for 1,504 leaves from 185 taxa were compiled from the literature (taxa and sources are given in Supplementary Information). Data were compiled for crop and non-crop taxa from a variety of growth conditions (direct sunlight, shade, irrigation, outdoors, growth chambers, and so on), but appeared to be biased towards sunlit leaves (513 sunlight/illuminated, 230 shade/cloudy, 761 not noted). Analyses included data from leaves that were not noted to be water stressed (and thus non-photosynthetic). The general results did not change when data were subsetted for various crop/non-crop plants, environmental conditions and growth conditions. Second, long-term photosynthetically weighted estimates for over 64 species were compiled from refs 16,37–43 (taxa are listed in the Supplementary Information). In this approach, leaf temperatures were estimated using a cellulose $\delta^{18}O$ model[44] parameterized with data for climate and cellulose $\delta^{18}O$ measured in tree wood[16,37–42] and graminoid leaves[43]. For both approaches, taxa were assigned a growth form (cushion, graminoid, herb, shrub, succulent or tree) using plant trait databases (BIEN[28] and plants.usda.gov).

Leaf trait and climate data

Compiled data. Leaf trait data comprising complete records for taxon, leaf type, projected area and dry mass were subsetted from the GLOPNET database[22], yielding a total of 301 individual leaf records (data are described in Supplementary Information). Most records also included stomatal conductance, but when they did not, it was calculated as the mean of the finest taxonomic resolution (species, genus or family) available in BIEN[28]. Additionally, LDMC was calculated as the mean of the finest taxonomic resolution (species, genus or family) available in BIEN[28]. To facilitate matching across databases, all taxon names were standardized using the Taxonomic Name Resolution Service[45]. Records without stomatal conductance or LDMC data were excluded, yielding a total of 138 individual leaf records. We also compiled photosynthesis temperature response data corresponding to genera or species of GLOPNET leaf traits. A total of 89 individual curves were compiled. A complete list of taxa and sources is provided in the Supplementary Information.

Climate data for GLOPNET leaf trait sites were compiled from multiple data sources. First, latitude and longitude were obtained for leaf trait sites from the primary sources listed in GLOPNET[22]. Second, site elevations were obtained from a 10 arc-minute WorldClim[46] grid. Third, site mean growing season temperature and relative humidity data were calculated from a global 10-min resolution gridded climatology[29] following the methodology of Michaletz *et al.*[3] Fourth, site solar irradiance and soil surface temperature data were obtained from microclim[30].

Measured data. We collected leaf thermal trait (leaf type, projected area, LMA, LDMC, and stomatal conductance) and leaf photosynthetic trait (T_{opt} and T_{90}) data

for nine species (including broad leaves and conifers) from five sites along an air temperature gradient from Los Alamos National Laboratory in New Mexico (2,175 m; 35.82° N, −106.31° W) to Gunnison National Forest in Colorado (3,370 m; 38.97° N, −107.04° W). To account for covariation of traits among leaves, all thermal and photosynthetic traits were measured for each leaf. Photosynthesis and stomatal conductance data were measured using a LI-COR LI-6400xt with a 6,400–88 Expanded Temperature Control Kit. For both conifers and broad leaves, leaves (not shoots) were inserted into the leaf chamber and the block temperature was reduced using ice water. Gas exchange data were collected once the block and leaf temperatures had stabilized. After each measurement, the block temperature was increased in 5 °C increments until it was as high as possible using heated water. In this way, we were able to measure gas exchange across a range of approximately 25 °C for each individual. All photosynthesis data were corrected to account for the leaf area enclosed in the LI-COR chamber. Stomatal conductance was taken as the average calculated from the temperature response curve. Data for herbaceous broad leaf species (*Artemisia tridentata*, *Chamerion angustifolium*, *Delphinium barbeyi*, *Ligusticum porteri*, *Potentilla gracilis*, *Valeriana occidentalis*, *Veratrum californicum*) were obtained from intact plants at Gunnison National Forest during June, 2015. Additional leaf traits were measured for each single broad leaf that was measured in the LI-COR chamber. Data for woody conifer species (*Pinus edulis* and *Juniperus monosperma*) were obtained from branches harvested from the south side of crown tops at Los Alamos National Laboratory in August 2015. To excise branches from the tree, braches were cut under water using an anvil-style pruner; any embolisms that may have been introduced during excision were removed by recutting branch ends in approximately 5 cm sections two or three times under water. Branches were stored outdoors standing in water, and were fully sun exposed until measurement. Additional traits were measured either for single or three leaves among many that were measured in LI-COR chamber.

Microlimate data were obtained from permanent weather stations installed at each site. For conifer sites, growing seasons were estimated based on the date of budbreak and the date of first freeze. For broad leaf sites, growing season length was estimated from site observations of snowmelt and snowfall dates. For all sites, growing season estimates agreed with independent estimates calculated from gridded climate data[29] following ref. 3.

Data analyses. To evaluate theoretical and empirical support for leaf thermoregulation, we compared leaf temperatures predicted by energy budgets to the point and $\delta^{18}O$ data described above (Fig. 2). Leaf temperatures were predicted using Supplementary Equations (16)–(25) based on ref. 47, parameterized for a global average leaf based on the leaf trait and microclimate data described above. This approach more accurately predicts leaf thermoregulation than the Penman approximation, for which accuracy decreases with leaf temperature excess (up to more than 30% error)[47–50]. Median trait and climate values were used and held constant. For the net radiation term (Supplementary Equation 3), we assumed the leaf was positioned horizontally with the sun directly overhead, the sky temperature was 20 °C cooler than air[51], leaf absorptance was taken as 0.47 (ref. 52), and leaf emissivity was taken as 0.98 (ref. 52). To solve the energy balance Supplementary Equations (16)–(25), we first identified roots of the quartic Supplementary Equation (18) using the function polyroot in the statistical software R (ref. 53), and selected the single real, physically realistic root as the solution[47]. Energy budget predictions for leaf temperature were compared to empirical data using the root mean squared error (r.m.s.e.) and a normalized root mean squared error (n.r.m.s.e.) where the r.m.s.e. was normalized by the range of minimum and maximum observed leaf temperatures. Since the relationship between leaf and air temperatures is non-linear, slopes and intercepts of the predicted data were quantified using ordinary least squares (OLS) regression across the range of air temperatures observed in empirical data using R. OLS regressions were also fit to empirical leaf and air temperature data. Following ref. 19, thermoregulation was quantified by comparing fitted slopes to hypothesized values of 0 (true homeothermy) and 1 (true poikilothermy). We also quantified thermoregulation using plots of leaf temperature excess ($T_l - T_a$) versus air temperature, where fitted slopes were compared with hypothesized values of −1 (true homeothermy) and 0 (true poikilothermy). To evaluate patterns of thermoregulation among plant growth forms, we compared (1) slopes and elevations of leaf temperature versus air temperature, and (2) elevations of leaf temperature excess versus air temperature. Pairwise tests for a common OLS slope were conducted using the package lsmeans in R. Pairwise tests for elevation were conducted using Kruskal–Wallace tests from base R with Tukey and Kramer (Nemenyi) post hoc tests from the PMCMR package in R.

To evaluate the trade-off predicted by equation (9), we compared species- or genus-level data for T_{90} and τ (Fig. 3). T_{90} data were calculated using Supplementary Equation (44) with quadratic parameters a, b and c estimated by fitting Supplementary Equation (41) to photosynthesis temperature response data (described above). Thermal time constants were calculated using equation (7) parameterized with global leaf trait and microclimate data (described above). Total leaf area was calculated from projected area assuming a flat plate geometry for broad leaves and a cylindrical geometry for needle leaves. Leaf characteristic dimension was taken as $L = 0.7\sqrt{A_p}$ (ref. 54), where A_p (m^2) is projected area. Leaf absorptance was taken as 0.6 for broad leaves and 0.7 for needle leaves[52]. Overall heat transfer coefficients (Supplementary Information) were calculated using site microclimate data (above) with air density calculated from a linear fit to data from 23 to 77 °C (refs 51,55), specific heat capacity of air taken as 1,007 J kg^{-1} K^{-1} (ref. 55), leaf emissivity taken as 0.96 (ref. 52), saturation vapour pressure calculated from a fourth-order polynomial fit to data from −10 to 70 °C (ref. 56), slopes of the saturation vapour pressure curve versus temperature calculated using a third-order polynomial fit to slopes from the previously described relationship, air pressure calculated as a function of site elevation (assuming sea-level pressure of 101,325 Pa and temperature of 288.15 K, lapse rate of 0.0065 K m^{-1}, and molar mass of air of 0.0289644 kg mol^{-1}), and the psychrometer constant calculated following ref. 51. All calculations assumed a wind velocity of 0.3 m s^{-1}, a value that is typical within plant canopies[51], and although variation in wind velocity can influence τ via boundary layer effects[57] (Supplementary Equations 5 and 6), the use of 0.3 m s^{-1} did not bias our results since changing wind velocity to 0.1 and 10 m s^{-1} had only a minimal effect on the fit of T_{90} versus τ (for literature data $r^2 = 0.59$, 0.59, and 0.56 at wind velocities of 0.1, 0.3 and 10 m s^{-1}, respectively; for our data $r^2 = 0.30$, 0.30, and 0.28 at wind velocities of 0.1, 0.3 and 10 m s^{-1}, respectively). To evaluate the predicted inverse relationship between T_{90} and τ, data were fit using non-linear regression of Supplementary Equation 50 using package nls() in R. Preliminary calculations using smaller subsets of data for which absorptance, width and wind velocity were available at species-, genus-, family- or site-level data did not change the general results.

To evaluate the sensitivity of time constants to variation in constituent leaf traits (Fig. 4), baseline time constants were first calculated using median values of traits from global traits and microclimate (described above). Individual trait values were then varied as the median ±0.5 median absolute deviation of each trait distribution (the same general results were observed when using median ±minimum and maximum observed trait values). In this way, sensitivity of the thermal time constant could be evaluated with respect to empirical variation in the constituent traits, as opposed to simply varying constituent trait averages by some fixed amount of the average (for example, ±20%). Boundary layer conductances were calculated assuming a flat plate geometry (Supplementary Equation 5) and a wind velocity of 0.3 m s^{-1}.

Received 2 December 2015; accepted 27 July 2016; published 22 August 2016; corrected 26 August 2016

References

1. Michaletz, S. T. *et al.* Plant thermoregulation: energetics, trait-environment interactions, and carbon economics. *Trends Ecol. Evol.* **30,** 714–724 (2015).
2. Mahan, J. R. & Upchurch, D. R. Maintenance of constant leaf temperature by plants—I. Hypothesis-limited homeothermy. *Environ. Exp. Bot.* **28,** 351–357 (1988).
3. Michaletz, S. T., Cheng, D., Kerkhoff, A. J. & Enquist, B. J. Convergence of terrestrial plant production across global climate gradients. *Nature* **512,** 39–43 (2014).
4. Cuny, H. E. *et al.* Woody biomass production lags stem-girth increase by over one month in coniferous forests. *Nat. Plants* **1,** 15160 (2015).
5. Yvon-Durocher, G. *et al.* Methane fluxes show consistent temperature dependence across microbial to ecosystem scales. *Nature* **507,** 488–491 (2014).
6. Williams, P. A. *et al.* Temperature as a potent driver of regional forest drought stress and tree mortality. *Nat. Clim. Change* **3,** 292–297 (2013).
7. Huxman, T. E., Turnipseed, A. A., Sparks, J. P., Harley, P. C. & Monson, R. K. Temperature as a control over ecosystem CO_2 fluxes in a high-elevation, subalpine forest. *Oecologia* **134,** 537–546 (2003).
8. Berry, J. & Bjorkman, O. Photosynthetic response and adaptation to temperature in higher plants. *Ann. Rev. Plant Physiol.* **31,** 491–543 (1980).
9. Slatyer, R. & Morrow, P. Altitudinal variation in the photosynthetic characteristics of snow gum, *Eucalyptus pauciflora* Sieb. Ex Spreng. I. Seasonal changes under field conditions in the Snowy Mountains area of south-eastern Australia. *Aust. J. Bot.* **25,** 1–20 (1977).
10. Korner, C. & Diemer, M. *In situ* photosynthetic responses to light, temperature and carbon dioxide in herbaceous plants from low and high altitude. *Funct. Ecol.* **1,** 179–194 (1987).
11. Yamori, W., Hikosaka, K. & Way, D. A. Temperature response of photosynthesis in C3, C4, and CAM plants: temperature acclimation and temperature adaptation. *Photosynth. Res.* **119,** 101–117 (2014).
12. Gates, D., Hiesey, W., Milner, H. & Nobs, M. Temperatures of *Mimulus* leaves in natural environments and in a controlled chamber. *Carnegie Inst. Wash. Yearb.* **63,** 418–430 (1964).
13. Linacre, E. T. A note on a feature of leaf and air temperatures. *Agric. Meteorol.* **1,** 66–72 (1964).
14. Linacre, E. T. Further notes on a feature of leaf and air temperatures. *Arch. Meteorol. Geophys. Bioklimatol. B* **15,** 422–436 (1967).
15. Upchurch, D. R. & Mahan, J. R. Maintenance of constant leaf temperature by plants—II. Experimental observations in cotton. *Environ. Exp. Bot.* **28,** 359–366 (1988).
16. Helliker, B. R. & Richter, S. L. Subtropical to boreal convergence of tree-leaf temperatures. *Nature* **454,** 511–514 (2008).
17. Potter, K., Davidowitz, G. & Woods, H. A. Insect eggs protected from high temperatures by limited homeothermy of plant leaves. *J. Exp. Biol.* **212,** 3448–3454 (2009).

18. Smith, W. K. & Carter, G. A. Shoot structural effects on needle temperatures and photosynthesis in conifers. *Am. J. Bot.* **75,** 496–500 (1988).
19. Huey, R. B. & Slatkin, M. Cost and benefits of lizard thermoregulation. *Q. Rev. Biol.* **51,** 363–384 (1976).
20. Rowland, L. *et al.* Modelling climate change responses in tropical forests: similar productivity estimates across five models, but different mechanisms and responses. *Geosci. Model Dev.* **8,** 1097–1110 (2015).
21. Reich, P. B., Walters, M. B. & Ellsworth, D. S. From tropics to tundra: global convergence in plant functioning. *Proc. Natl Acad. Sci.* **94,** 13730–13734 (1997).
22. Wright, I. J. *et al.* The worldwide leaf economics spectrum. *Nature* **428,** 821–827 (2004).
23. Falster, D. S. *et al.* Lifetime return on investment increases with leaf lifespan among 10 Australian woodland species. *New Phytol.* **193,** 409–419 (2012).
24. Blonder, B., Violle, C., Bentley, L. P. & Enquist, B. J. Venation networks and the origin of the leaf economics spectrum. *Ecol. Lett.* **14,** 91–100 (2011).
25. Ball, M., Cowan, I. & Farquhar, G. Maintenance of leaf temperature and the optimisation of carbon gain in relation to water loss in a tropical mangrove forest. *Funct. Plant Biol.* **15,** 263–276 (1988).
26. Slot, M., Garcia, M. N. & Winter, K. Temperature response of CO_2 exchange in three tropical tree species. *Funct. Plant Biol.* **43,** 468–478 (2016).
27. Slot, M. & Winter, K. in *Tropical Tree Physiology Adaptations and Responses in a Changing Environment* (eds Goldstein, G. & Santiago, S. L.) 385–412 (Springer International, 2016).
28. *The Botanical Information and Ecology Network* (BIEN, 2016); http://bien.nceas.ucsb.edu/bien/
29. New, M., Lister, D., Hulme, M. & Makin, I. A high-resolution data set of surface climate over global land areas. *Climate Res.* **21,** 1–25 (2002).
30. Kearney, M. R., Isaac, A. P. & Porter, W. P. microclim: Global estimates of hourly microclimate based on long-term monthly climate averages. *Sci. Data* **1,** 140006 (2014).
31. Paw U, K. T. A theoretical basis for the leaf equivalence point temperature. *Agricult. Meteorol.* **30,** 247–256 (1984).
32. Kikuzawa, K. & Lechowicz, M. J. Toward synthesis of relationships among leaf longevity, instantaneous photosynthetic rate, lifetime leaf carbon gain, and the gross primary production of forests. *Am. Nat.* **168,** 373–383 (2006).
33. Ehleringer, J. R. Changes in leaf characteristics of species along elevational gradients in the Wasatch Front, Utah. *Am. J. Bot.* **75,** 680–689 (1988).
34. Moles, A. T. *et al.* Which is a better predictor of plant traits: temperature or precipitation? *J. Veg. Sci.* **25,** 1167–1180 (2014).
35. Leigh, A. *et al.* Do thick leaves avoid thermal damage in critically low wind speeds? *New Phytol.* **194,** 477–487 (2012).
36. Vogel, S. Leaves in the lowest and highest winds: temperature, force and shape. *New Phytol.* **183,** 13–26 (2009).
37. Song, X., Barbour, M. M., Saurer, M. & Helliker, B. R. Examining the large-scale convergence of photosynthesis-weighted tree leaf temperatures through stable oxygen isotope analysis of multiple data sets. *New Phytol.* **192,** 912–924 (2011).
38. Barbour, M. M., Andrews, T. J. & Farquhar, G. D. Correlations between oxygen isotope ratios of wood constituents of *Quercus* and *Pinus* samples from around the world. *Funct. Plant Biol.* **28,** 335–348 (2001).
39. Saurer, M., Schweingruber, F., Vaganov, E. A., Shiyatov, S. G. & Siegwolf, R. Spatial and temporal oxygen isotope trends at the northern tree-line in Eurasia. *Geophys. Res. Lett.* **29,** 7-1–7-4 (2002).
40. Evans, M. N. & Schrag, D. P. A stable isotope-based approach to tropical dendroclimatology. *Geochim. Cosmochim. Acta* **68,** 3295–3305 (2004).
41. Poussart, P. F., Evans, M. N. & Schrag, D. P. Resolving seasonality in tropical trees: multi-decade, high-resolution oxygen and carbon isotope records from Indonesia and Thailand. *Earth Planet. Sci. Lett.* **218,** 301–316 (2004).
42. Poussart, P. F. & Schrag, D. P. Seasonally resolved stable isotope chronologies from northern Thailand deciduous trees. *Earth Planet. Sci. Lett.* **235,** 752–765 (2005).
43. Flanagan, L. B. & Farquhar, G. D. Variation in the carbon and oxygen isotope composition of plant biomass and its relationship to water-use efficiency at the leaf- and ecosystem-scales in a northern Great Plains grassland. *Plant Cell Environ.* **37,** 425–438 (2014).
44. Barbour, M. M. & Farquhar, G. D. Relative humidity- and ABA-induced variation in carbon and oxygen isotope ratios of cotton leaves. *Plant Cell Environ.* **23,** 473–485 (2000).
45. Boyle, B. *et al.* The taxonomic name resolution service: an online tool for automated standardization of plant names. *BMC Bioinform.* **14,** 1–15 (2013).
46. Hijmans, R. J., Cameron, S. E., Parra, J. L., Jones, P. G. & Jarvis, A. Very high resolution interpolated climate surfaces for global land areas. *Int. J. Climatol.* **25,** 1965–1978 (2005).
47. Paw U, K. T. Mathematical analysis of the operative temperature and energy budget. *J. Therm. Biol.* **12,** 227–233 (1987).
48. Tracy, C. R. *et al.* Errors resulting from linear approximations in energy balance equations. *J. Therm. Biol.* **9,** 261–264 (1984).
49. Paw U, K. T. & Gao, W. Applications of solutions to non-linear energy budget equations. *Agric. Forest Meteorol.* **43,** 121–145 (1988).
50. Widmoser, P. A discussion on and alternative to the Penman–Monteith equation. *Agric. Water Manag.* **96,** 711–721 (2009).
51. Jones, H. G. *Plants and Microclimate: A Quantitative Approach to Environmental Plant Physiology* (Cambridge Univ. Press, 2014).
52. Gates, D. M. *Biophysical Ecology* (Springer-Verlag, 1980).
53. R Core Team *R: A Language and Environment for Statistical Computing* (R Foundation for Statistical Computing, 2014).
54. Campbell, G. S. & Norman, J. M. *An Introduction to Environmental Biophysics* (Springer, 1998).
55. Bergman, T. L., Lavine, A. S., Incropera, F. P. & DeWitt, D. P. *Fundamentals of Heat and Mass Transfer* 7th edn (John Wiley, 2011).
56. Goff, J. A. & Gratch, S. Low-pressure properties of water from −160 to 212 °F. *Trans. Am. Soc. Heat. Vent. Eng.* **51,** 125–164 (1946).
57. Michaletz, S. T. & Johnson, E. A. Foliage influences forced convection heat transfer in conifer branches and buds. *New Phytol.* **170,** 87–98 (2006).

Acknowledgements

This paper is dedicated to the memory of Dr David M. Gates, who began studying the thermoregulation and energy budgets of leaves more than a half century ago. The authors thank B. Blonder for providing thoughtful comments on an earlier version of the paper, L. Stockton for helping collect leaf trait and gas exchange data, H. Adams, A. Collins, T. Dickman, C. Grossiord, A. Henderson, J. Reithel and S. Sevanto for providing meteorological and phenological data, and J. Finch and J. Draper for supplying the *Brachypodium distachyon* image used in Fig. 1. S.T.M. was supported by a Director's Fellowship from the Los Alamos National Laboratory. S.T.M., M.D.W., J.Z., M.K. and B.J.E. were supported by NSF MacroSystems award 1065861. B.R.H. was supported under NSF award IOS-0950998 and NSF MacroSystems award 1241873. N.G.M. was supported by SUMO and NGEE-Tropics support from the Department of Energy, Office of Science. B.J.E. was supported by a fellowship from the Aspen Center for Environmental Studies.

Author contributions

S.T.M., M.D.W., N.G.M., J.Z., M.K., B.R.H. and B.J.E. compiled data, developed theory, performed analyses and wrote the paper.

Additional information

Supplementary information is available for this paper. Reprints and permissions information is available at www.nature.com/reprints. Correspondence and requests for materials should be addressed to S.T.M.

Competing interests

The authors declare no competing financial interests.

Corrigendum: The energetic and carbon economic origins of leaf thermoregulation

Sean T. Michaletz, Michael D. Weiser, Nate G. McDowell, Jizhong Zhou, Michael Kaspari, Brent R. Helliker and Brian J. Enquist

Nature Plants **2,** 16129 (2016); published 22 August 2016; corrected 26 August 2016.

In the version of this Article originally published, the affiliation for Nate G. McDowell was incorrect. This has now been corrected.